Sintering behavior and microwave dielectric properties of V5+ substituted Li3Mg2SbO6 ceramics

Article *in* Journal of Materials Science: Materials in Electronics · August 2019

DOI: 10.1007/s10854-019-01819-7

CITATIONS
3

READS
86

8 authors, including:

Guoguang Yao
Xi'an University of Posts and Telecommunications
33 PUBLICATIONS **285** CITATIONS
SEE PROFILE

Wei Ren
Xi'an University of Posts and Telecommunications
72 PUBLICATIONS **599** CITATIONS
SEE PROFILE

Peng Liu
Shaanxi Normal University
273 PUBLICATIONS **5,054** CITATIONS
SEE PROFILE

Journal of Materials Science: Materials in Electronics
https://doi.org/10.1007/s10854-019-01819-7

Sintering behavior and microwave dielectric properties of V^{5+} substituted $Li_3Mg_2SbO_6$ ceramics

Cui-jin Pei[1] · Yang Li[1] · Cai-dan Hou[1] · Bo-xuan Xie[1] · Guo-guang Yao[1,2] · Wei Ren[1] · Zhao-yu Ren[2] · Peng Liu[3]

Received: 3 May 2019 / Accepted: 3 July 2019

Abstract
The $Li_3Mg_2(Sb_{1-x}V_x)O_6$ ($0.01 \le x \le 0.04$) ceramics have been synthesized by the solid-state reaction method. The effects of V^{5+} ion substitution on the sinterability, phase composition and microwave dielectric properties of $Li_3Mg_2(Sb_{1-x}V_x)O_6$ ceramics were investigated. The dehiscence and secondary phase in $Li_3Mg_2SbO_6$-based ceramics could be effectively inhibited by partial substitution of V^{5+} on the Sb^{5+} sites. The optimum microwave dielectric properties ($\varepsilon_r = 11.2$, Qxf = 54,700 GHz, $\tau_f = -20$ ppm/°C) were obtained for $Li_3Mg_2(Sb_{1-x}V_x)O_6$ ($x = 0.03$) ceramics sintered at 1250 °C. The ε_r of $Li_3Mg_2(Sb_{0.97}V_{0.03})O_6$ ceramics was mainly depended on ionic polarizability as well as density, whereas its Qxf was strongly dominated by average grain size.

1 Introduction

With the rapid development of wireless communication, microwave dielectric ceramics have been extensively investigated as various components for wireless communication, including substrates, antennas, and resonators [1, 2]. Microwave dielectric materials for application as advanced substrate must have a low dielectric constant (ε_r), a high quality factor ($Q \times f$), and a near zero temperature coefficient of resonant frequency (τ_f) to reduce signal delay, enhance frequency selectivity and improve temperature stability, respectively [3, 4]. Moreover, the recent progresses in 5th generation mobile communication systems and microelectronic technologies have urged scientists to develop novel microwave substrate materials owing above mentioned high performances [5].

Recently, $Li_3Mg_2NbO_6$-based ceramics with orthorhombic structure have been widely studied due to their excellent microwave dielectric characteristics [6–10]. $Li_3Mg_2SbO_6$ has the same structure as that of $Li_3Mg_2NbO_6$, as reported by West et al. [11]. However, there are few reports on the microwave dielectric properties of single-phase $Li_3Mg_2SbO_6$ ceramics, which is due to its dehiscence during sintering caused by the secondary phase SbO_x in it [12]. The dehiscent drawback of $Li_3Mg_2SbO_6$ ceramics limited its practical application in microwave devices. Ionic substitution is an effective method to improve the sinterability and microwave dielectric properties of ceramics by forming a solid solution [13–15]. Recently, Zhang et al. [16] reported that partial Sb substitution for Nb in $Li_3Mg_2(Nb_{1-x}Sb_x)O_6$ ($0.02 \le x \le 0.08$) could optimize its τ_f value. Our pervious study showed that the partial Ba substitution for Sr in SrV_2O_6 could effectively inhibit the dehiscence of SrV_2O_6-based ceramics [17].Wang et al. successfully decreased the sintering temperature of $Li_3Mg_2NbO_6$ ceramics by partial V substitution for Nb [18]. These results urged us to prepare $Li_3Mg_2SbO_6$-basic ceramics without dehiscence by V substitution for Sb. In present work, the $Li_3Mg_2(Sb_{1-x}V_x)O_6$ ($0.01 \le x \le 0.04$) solid solutions were prepared and the relationships among the sintering behavior, microstructure, phase composition and microwave dielectric properties of $Li_3Mg_2(Sb_{1-x}V_x)O_6$ were studied.

2 Experimental procedure

$Li_3Mg_2Sb_{1-x}V_xO_6$ ($0.01 \le x \le 0.04$) ceramics were prepared through the standard solid-state reaction method. Predried raw materials Li_2CO_3, MgO, Sb_2O_3 and V_2O_5 (all

✉ Guo-guang Yao
yaoguoguang@xupt.edu.cn

[1] School of Science, Xi'an University of Posts and Telecommunications, Xi'an 710121, China

[2] Institute of Photonics & Photon-Technology, Northwest University, Xi'an 710069, China

[3] College of Physics and Information Technology, Shaanxi Normal University, Xi'an 710062, China

Published online: 09 July 2019

purity > 99.9%) were weighted according to stoichiometric mixtures $Li_3Mg_2Sb_{1-x}V_xO_6$ and ball-milled in a nylon jar with ethanol and agate spheres for 8 h. The obtained slurries were dried, crushed and calcined at 875 °C for 4 h. The calcined powders were re-milling for 8 h, dried, mixed with 5 wt % polyvinyl alcohol (PVA) as an adhesive, and granulated. The granulated powders were pressed into cylindrical pellets (10 mm × 5 mm). The green pellets were sintered at 1175–1275 °C for 5 h in air.

The bulk density of the sintered samples was measured with Archimedes' method. The crystalline phases were characterized by X-ray powder diffraction (XRD) with Cu Kα radiation (RigakuD/MAX2550, Tokyo, Japan). The surface microstructure of sintered specimens was revealed using scanning electron microscope (SEM, Fei Quanta 200, Eindhoven, Holland) and the grain size was estimated by the image analysis software (Image Tool for Windows version 3.00, Microsoft, Redmond, WA). The microwave dielectric properties of sintered samples were measured with the $TE_{01\delta}$ shielded cavity method using a network analyzer (ZVB20, Rohde & Schwarz, Germany). The τ_f was calculated using the following Eq. (1):

$$\tau_f = \frac{f - f_0}{f_0 \times (T - T_0)} \times 10^6 \quad (1)$$

where f and f_0 are the resonant frequency at T (80 °C) and T_0 (20 °C), respectively.

3 Results and discussion

Figure 1 illustrates the XRD patterns for $Li_3Mg_2(Sb_{1-x}V_x)O_6$ ($0.01 \le x \le 0.04$) ceramics sintered at 1250 °C. The diffraction peaks of all specimens could be well indexed according to the JCPDS 86-0345 card. And no obvious secondary phase was detected throughout the substitution range from 0.01 to 0.04. Therefore, all specimens crystallized in a single phase with orthorhombic structure and Fddd space group. In addition, the phase composition of the $Li_3Mg_2Sb_{0.7}V_{0.3}O_6$ ceramics fired at different temperatures were also analyzed and characterized with the XRD patterns, as shown in Fig. 2. It could found in Fig. 2 that all samples also exhibited pure phase $Li_3Mg_2SbO_6$ without an obvious secondary phase. The results show that secondary phase in $Li_3Mg_2SbO_6$-based ceramics could be effectively inhibited by partial substitution of V^{5+} on the Sb^{5+} sites [12].

The bulk density of $Li_3Mg_2(Sb_{1-x}V_x)O_6$ ($0.01 \le x \le 0.04$) ceramics as a function of sintering temperature is illustrated in Fig. 3. The changes of the bulk densities are similar for all the specimens sintered at different temperatures. The bulk density for each composition initially increased and then decreased with the increment of sintering temperature. And the optimum sintering temperature for each composition

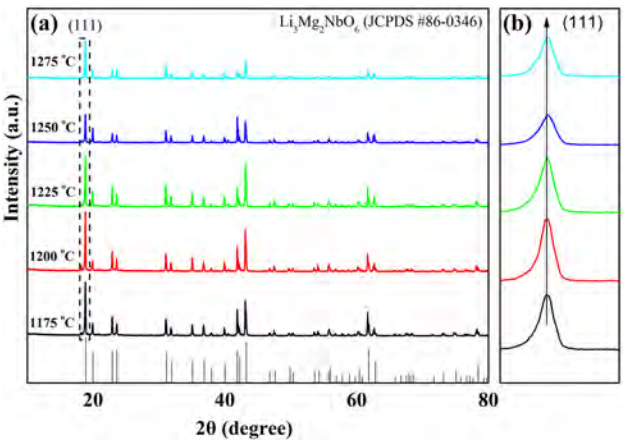

Fig. 2 XRD patterns for $Li_3Mg_2Sb_{0.97}V_{0.03}O_6$ ceramics sintered at different temperatures

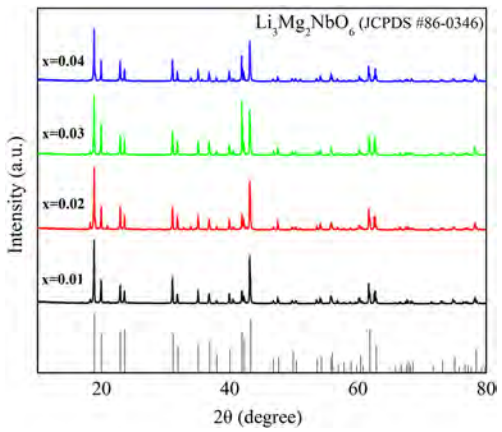

Fig. 1 XRD patterns of $Li_3Mg_2(Sb_{1-x}V_x)O_6$ ($0.01 \le x \le 0.04$) ceramics sintered at 1250 °C

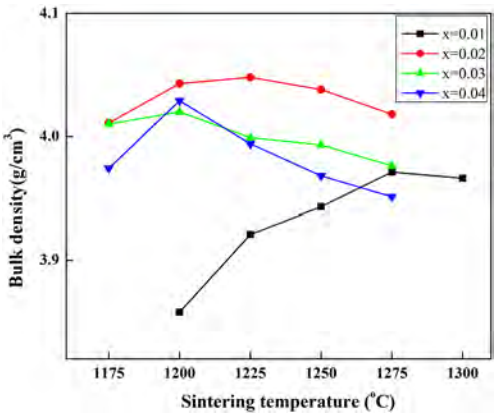

Fig. 3 Bulk density of $Li_3Mg_2(Sb_{1-x}V_x)O_6$ ($0.01 \le x \le 0.04$) ceramics as a function of sintering temperature

decreased from 1275 to 1200 °C with increasing x from 0.01 to 0.04, indicating that partial V substitution for Sb could reduce the sintering temperature of $Li_3Mg_2SbO_6$-based ceramics. The similar phenomena are also reported in other ceramics [19, 20].

Figure 4 illustrates the typical SEM micrographs of $Li_3Mg_2Sb_{0.97}V_{0.03}O_6$ specimens sintered at 1200–1275 °C. As shown in Figs. 4a–c, the pores gradually decreased and the grain size grew as the sintering temperature increased from 1200 to 1250 °C. The specimen fired at 1250 °C exhibited a dense microstructure with an average grain size about 18.7 μm. However, for the specimen fired at 1275 °C, partial melted grains and fuzzy grain boundaries appeared due to over-sintering, as shown in Fig. 4d, which would deteriorate dielectric properties of ceramics [21].

Figure 5 exhibits the values of ε_r for $Li_3Mg_2(Sb_{1-x}V_x)O_6$ ($0.01 \le x \le 0.04$) ceramics sintered at 1175–1275 °C. At microwave region the ε_r is mainly determined by the intrinsic causes, such as ionic polarizability, and extrinsic causes, such as phase constitution and porosity [22]. For $x = 0.01$ and 0.02 samples, the ε_r values firstly ascended and then declined with increasing sintering temperature, which presented a similar variation tendency with density. Thus, the ε_r values for $x = 0.01$ and 0.02 samples were mainly dominated by density. Whereas in the samples for $x = 0.03$ and 0.04, the variation trend between ε_r and sintering temperature

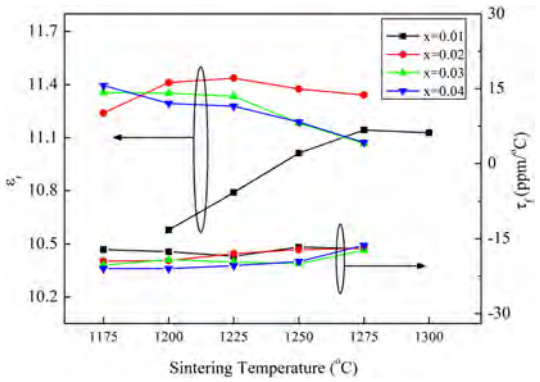

Fig. 5 Variation of ε_r and τ_f values of $Li_3Mg_2(Sb_{1-x}V_x)O_6$ ($0.01 \le x \le 0.04$) ceramics sintered at various temperatures for 5 h

exhibited somewhat difference as that of density vs sintering temperature, indicating that some other factors should be considered except density. The similar phenomena were also observed in other V-containing ceramics [23, 24]. Based on Clausius–Mossotti equation [22], the ε_r is in direct proportion to ionic polarizability and in inverse proportion to molecular volume. In our case, the sum ionic polarizability of specimen decreased at higher sintering temperature, which is due to the evaporation of V_2O_5 during the sintering process [23, 24]. Moreover, as seen in Fig. 2b, there is no

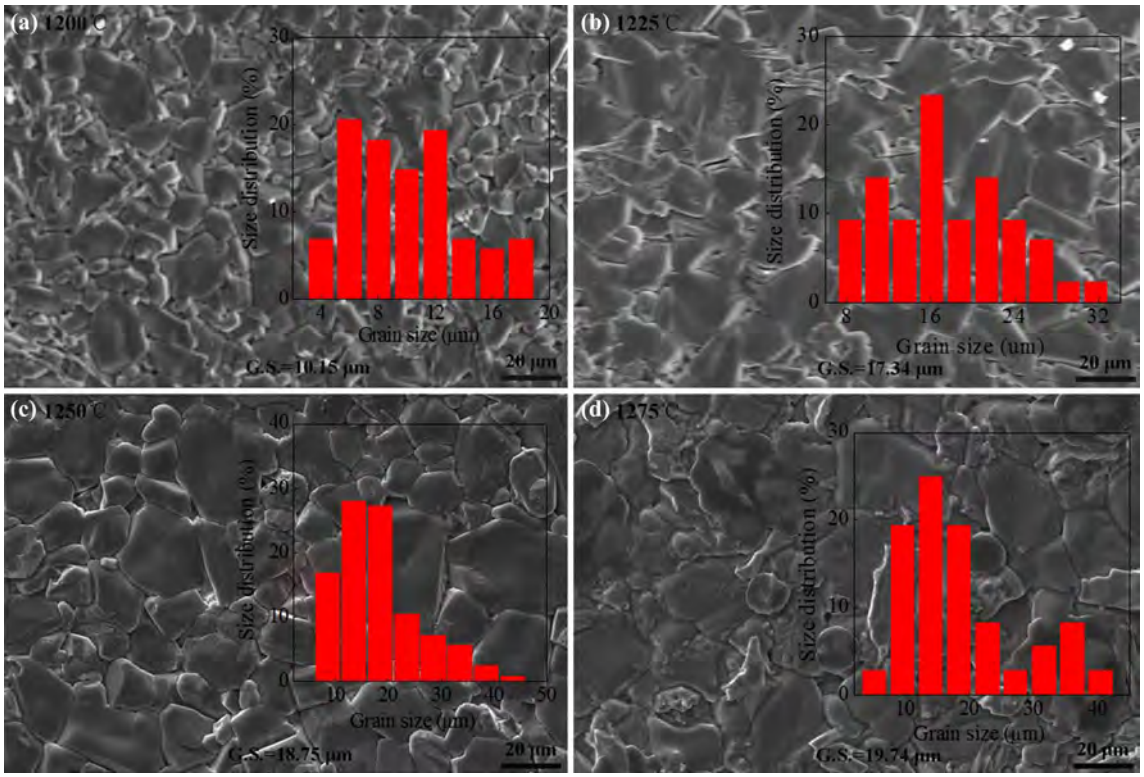

Fig. 4 Typical SEM micrographs of $Li_3Mg_2Sb_{0.97}V_{0.03}O_6$ ceramics fired at different temperatures

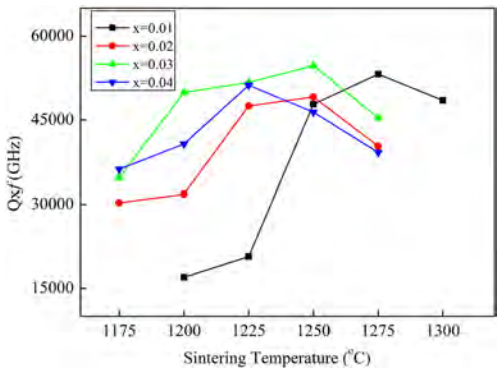

Fig. 6 Qxf curves of $Li_3Mg_2(Sb_{1-x}V_x)O_6$ ($0.01 \le x \le 0.04$) ceramics fired at different temperatures

obvious shift of diffraction peak with increasement of firing temperature, indicating no obvious change of molecular volume. Thus, the ε_r of $Li_3Mg_2(Sb_{0.97}V_{0.03})O_6$ ceramics was mainly depended on ionic polarizability as well as density. For the samples with $0.01 \le x \le 0.04$, the maximum ε_r values slightly fluctuated in the range of 11.1 to 11.4, implying that the ε_r value is limited dependent on content x. As shown in Fig. 5, the τ_f value showed the relative independence on content x and sintering temperature, and it remained stable around − 20 ppm/°C, because no secondary phase and structure change existed [25].

The Qxf values of $Li_3Mg_2(Sb_{1-x}V_x)O_6$ ($0.01 \le x \le 0.04$) ceramics are plotted as a function of sintering temperature in Fig. 6. The Qxf of microwave dielectric ceramics is greatly affected by extrinsic factors such as average grain size, relative density, secondary phase [26]. Unlike density, the maximum Qxf values for all samples except $x = 0.1$ were obtained at the temperatures somewhat higher than their densification temperatures as illustrated in Fig. 3, indicating that other factors influencing the Qxf values should be considered as discussed below. Considering the secondary phase could be neglected as confirmed by aforementioned XRD analysis. Therefore, the average grain size was considered to be the key factor affected the Qxf values. As displayed in Fig. 4a–c, the average grain size increased from 10.1 to 18.7 μm as sintering temperature increased from 1175 to 1250 °C, resulting in the enhancement of Qxf values for $Li_3Mg_2(Sb_{0.97}V_{0.03})O_6$ ceramics. This is due to that the bigger grain size means less grain boundary defects and thus high Qxf value [27]. The over-sintering at 1275 °C might be responsible for the deterioration of Qxf, as seen in Fig. 4d. The highest Qxf values (54,700 GHz) were obtained for the $x = 0.03$ sample sintered at 1250 °C. Altogether, the $Li_3Mg_2(Sb_{0.97}V_{0.03})O_6$ ceramics sintered at 1250 °C owned with optimum microwave dielectric properties: $\varepsilon_r = 11.2$, Qxf = 54,700 GHz (at 10.3 GHz), $\tau_f = -20$ ppm/°C.

4 Conclusion

$Li_3Mg_2(Sb_{1-x}V_x)O_6$ ($0.01 \le x \le 0.04$) ceramics have been prepared through the conventional solid-state reaction route, and their sinterability, phase constitution and microwave dielectric performances were studied. The sinterability and phase purity of $Li_3Mg_2SbO_6$-based ceramics could be effectively improved by partial substitution of V^{5+} on the Sb^{5+} sites. The $Li_3Mg_2(Sb_{0.97}V_{0.03})O_6$ ceramics sintered at 1250 °C for 5 h had optimum microwave dielectric properties: $\varepsilon_r = 11.2$, Qxf = 54,700 GHz (at 10.3 GHz), $\tau_f = -20$ ppm/°C. The ε_r was mainly depended on ionic polarizability as well as density, whereas its Qxf was strongly affected by average grain size.

Acknowledgements This work is supported by the National Natural Science Foundation of China (Grant No. 51402235). China's Postdoctoral Science Fund (Grant No. 2015M582696), and by Shaanxi Province Postdoctoral Science Foundation. Shaan xi Province Department Education (No. 18JK0711).

References

1. H.T. Wu, E.S. Kim, J. Alloys Compd. **669**, 134 (2016)
2. Y.H. Zhang, J.J. Sun, N. Dai, Z.C. Wu, H.T. Wu, C.H. Yang, J. Eur. Ceram. Soc. **39**, 1127 (2019)
3. M.T. Sebastian, R. Ubic, H. Jantunen, Int. Mater. Rev. **60**, 392 (2015)
4. X.K. Lan, J. Li, Z.Y. Zou, G.F. Fan, W.Z. Lu, W. Lei, J. Eur. Ceram. Soc. **39**, 2360 (2019)
5. K.C. Feng, P.Y. Chen, P.H. Wu, C.S. Chen, C.S. Tu, J. Alloys Compd. **765**, 75 (2018)
6. P. Zhang, K.X. Sun, M. Xiao, Z.T. Zheng, J. Am. Ceram. Soc. **102**, 4127 (2019)
7. C.F. Xing, J.X. Bi, H.T. Wu, J. Alloys Compd. **719**, 58 (2017)
8. P. Zhang, L. Liu, M. Xiao, Y.G. Zhao, J. Mater. Sci. Mater. Electron. **28**, 12220 (2017)
9. T.W. Zhang, R.Z. Zuo, C. Zhang, Mater. Res. Bull. **68**, 109 (2015)
10. L.L. Yuan, J.J. Bian, Ferroelectrics **387**, 123 (2009)
11. M. Castellanos, J.A. Gard, A.R. West, J. Appl. Crystallogr. **15**, 116 (1982)
12. G.G. Yao, C.J. Pei, Z.Y. Ren, P. Liu, J. Mater. Sci. Mater. Electron. **29**, 9979 (2018)
13. C. Zhang, R.Z. Zuo, J. Zhang, Y. Wang, J. Am. Ceram. Soc. **98**, 702 (2015)
14. S.H. Wee, D.W. Kim, S.I. Yoo, K.S. Hong, Jpn. J. Appl. Phys. **43**, 3511 (2004)
15. Y.H. Zhang, H.T. Wu, J. Am. Ceram. Soc. **102**, 4092 (2019)
16. P. Zhang, S.X. Wu, X. Xiao, J. Alloys Compd. **766**, 498 (2018)
17. G.G. Yao, C.J. Pei, P. Liu, H.Y. Xing, B.C. Liang, J. Mater. Sci. Mater. Electron. **28**, 13283 (2017)
18. G. Wang, H.W. Zhang, Y. Yang, C. Liu, Ceram. Int. **44**, 19295 (2018)
19. F. Zhao, H. Zhuang, Z.X. Yue, Z.L. Gui, L.T. Li, Mater. Lett. **61**, 3466 (2007)
20. J. Wang, Z.X. Yue, Z.L. Gui, L.T. Li, J. Alloys Compd. **392**, 263 (2005)
21. M. Valant, D. Suvorov, Mater. Chem. Phys. **79**, 104 (2003)
22. R. Shannon, J. Appl. Phys. **73**, 348 (1993)

23. G.G. Yao, P. Liu, X.G. Zhao, J.P. Zhoua, H.W. Zhang, J. Eur. Ceram. Soc. **34**, 2983 (2014)
24. B. Li, L. Qiu, J.W. Tian, J. Alloys Compd. **767**, 797 (2018)
25. E.L. Colla, I.M. Reaney, N. Setter, J. Appl. Phys. **74**, 3414 (1993)
26. S.R. Kiran, V.R.K. Murthy, V. Subramanian, B.S. Murty, J. Am. Ceram. Soc. **95**, 1973 (2012)
27. J.D. Breeze, J.M. Perkins, D.W. McComb, N.M. Alford, J. Am. Ceram. Soc. **92**, 671 (2009)